An Improved Multigrid Technique for Quasi-TEM Analysis of a Microstrip Embedded in an Inhomogeneous Anisotropic Medium

Ching-Long Tsai and Way-Seen Wang, *Member, IEEE*

***Abstract*—An improved multigrid technique for the quasi-TEM analysis of a microstrip line embedded in an inhomogeneous anisotropic dielectric medium is presented. A general finite-difference form for the inhomogeneous anisotropic medium is derived by the finite-volume discretization of Gauss' theorem. By the analogy between the quasi-TEM and the steady current problems, this general form can be interpreted by Kirchhoff's current law. Then, the electric potential distribution in this complicated dielectric structure can be regarded as that on a resistive network, which makes the formulation easier. The resulting matrix equation for the potential distribution on the finest grid is solved by the improved multigrid iteration, where the coarse-grid operator is derived directly from the finest grid operator by the help of an equivalent resistive network. Three numerical examples show that the convergence rate is hardly dependent of the number of unknowns and the complexity of the dielectric media. Moreover, the numerical results are in good agreement with those by the other method when special cases are considered.**

***Index Terms*—Microstrip, multigrid, quasi-TEM.**

I. Introduction

QUASI-TEM analysis, which includes the calculation of capacitance and effective dielectric constant of a single or multiple conductor microstrip transmission line, is of great importance in the design of microwave integrated-circuit components, and therefore, has received a lot of attention. Recently, the quasi-TEM analysis is also essential in the study of integrated electro-optic modulation. Once the electric field distribution within the waveguiding region is obtained, the drive voltage of the modulator can be easily estimated. Hence, many computational methods have been proposed for the quasi-TEM analysis. Among the methods that have been used often are the conformal mapping method [1], [2], the boundary-element method [3], [4], the mode-matching method [5], the spectral-domain method [6], the moment method [7], [8], etc. However, each standard method is suitable only for a specific type of microstrip line structure. When a planar structure made of inhomogeneous anisotropic dielectric medium is to be analyzed, all the methods become too complicated to be widely applicable. Hence, the conventional finite-difference method [9]–[13] is then a possible choice for such a complicated problem.

A finite-difference solution basically involves the following steps:

1) deciding the governing equation, which can be a differential equation or an integral equation;
2) using a vertex-centered grid or a cell-centered grid [14] to discretize the computational domain into a finite set of grid points;
3) transforming the governing equation and the boundary conditions into finite-difference forms at each node, which gives rise to a set of linear equations;
4) solving these linear equations to get the numerical solutions on the nodes.

Many authors [9]–[13] use the vertex-centered grid to discretize the computational domain and convert the differential equation into finite-difference form at each grid point by replacing the derivatives by truncated Taylor's series. However, the normal derivative of the electric potential is discontinuous at the interface between two different dielectric media. Hence, this strategy is difficult to be implemented if there are two different dielectric media between two adjacent grid points.

In this paper, a finite-volume discretization of the integral equation on a cell-centered grid, which preserves the conservation of the electric flux, is used in the analysis of inhomogeneous anisotropic structure. The dielectric constant between two adjacent grid points is allowed to be discontinuous, which makes this strategy more flexible in constructing computational grid points. Owing to the close analogy between quasi-static and steady current problems, the derived general finite-difference form can be illustrated by a simple, but meaningful, resistive network.

To solve the matrix equation derived by discretization, two methods are commonly used. The first choice, is obviously the Gauss elimination method, which is also known as a direct method. However, this method is computationally intensive and can be prone to accumulated truncation error when the matrix size is large. Hence, several authors [9]–[13] adopt alternative choices, namely, the iteration methods such as the Gauss–Seidel (GS), red–black GS, and successive over-relaxation techniques. However, these conventional iteration methods all suffered from poor convergence because the oscillating errors can be effectively eliminated while the smooth er-

Manuscript received July 15, 1996; revised November 21, 1996. This work was support by the National Science Council, Taipei, Taiwan, R.O.C. under Contract NCS85-2215-E-002-009.

The authors are with the Department of Electrical Engineering, National Taiwan University, Taipei 10617, Taiwan, R.O.C.

Publisher Item Identifier S 0018-9480(97)02907-4.

rors cannot [14]–[20]. Recently, the multigrid method has been discussed in much of the mathematical literature [14]–[20], which shows that it is a powerful technique for iteration. The reported results show that different frequency components of the error can be damped separately by iterating on grids of various sizes, and, therefore, give rise to a much faster overall rate of convergence than iterating on the conventional single grid. To know more about the related work, several science databases such as Science Citation Index and Compendex have been searched. Unfortunately, no detailed application of the multigrid method in the quasi-TEM analysis of an inhomogeneous anisotropic medium has been reported so far. It then becomes of great interest to investigate how the multigrid method can be used or modified to overcome the poor convergence drawbacks mentioned previously.

To demonstrate the merit of the multigrid method in the field calculation, in this paper, the authors will directly cope with the calculation of an inhomogeneous anisotropic medium and leave the homogeneous isotropic calculation as a special case for data verification. For the multigrid calculation, a coarse-grid operator and a fine-grid operator for evaluating the data points must be efficiently used. When the medium is homogeneous, these two operators are essentially the same. For an inhomogeneous medium, the coarse-grid must be modified, for example, by the variational approach [16]. However, the calculation involved is too much to be time efficient [19]. In this paper, the general finite-difference form derived by finite-volume discretization is also applied in finding the coarse-grid operator directly from the existing fine-grid operator by the help of an equivalent resistive network, so a lot of coarse-grid operator calculations can be eliminated. Thus, the overall computation time is greatly reduced by the use of the multigrid iteration scheme and the resistive network analogy in finding the coarse-grid operator.

This paper is organized as follows. Section II describes the governing equations of the quasi-TEM problem. Section III describes the discretization of the computational domain. Section IV shows the derivation of the general finite-difference form by the finite-volume discretization method. Section V gives the network analogy of the finite-volume discretization and its application. The multigrid algorithm and the coarse-grid operator are described in Section VI. In Section VII, three examples are given for the demonstration of the capability of the present method. Results are then summarized in a brief conclusion.

II. Governing Equations for Potential Distribution

The problem to be considered is depicted as shown in Fig. 1. A rectangular outer conductor encloses a structure consisting of an infinitely thin inner conductor embedded in an inhomogeneous anisotropic dielectric medium. This structure is assumed to be uniform in the z-direction. Under the assumption that the mode of propagation is quasi-TEM, the field distribution in this structure is a two-dimensional (2-D) electrostatic problem in the x–y-plane. The inhomogeneous anisotropic effect of the dielectric medium is described by the

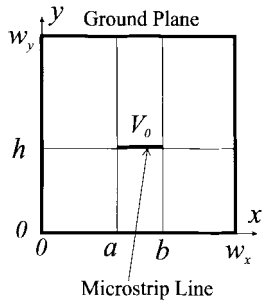

Fig. 1. Microstrip line embedded in an inhomogeneous anisotropic dielectric medium.

tensor

$$[\varepsilon] = \begin{bmatrix} \varepsilon_x(x, y) & 0 \\ 0 & \varepsilon_y(x, y) \end{bmatrix} \tag{1}$$

where ε_x and ε_y, dielectric constants, are assumed to be blockwise smooth in the computational domain. The normal vectors on the interfaces where the dielectric constants pose discontinuities are all assumed to be parallel to the x- or y-axis.

The governing equation for the electric potential distribution $\phi(x, y)$ in the 2-D inhomogeneous anisotropic dielectric region can be written as the partial differential equation

$$\nabla \cdot \left[-\hat{a}_x \varepsilon_x(x, y) \frac{\partial \phi(x, y)}{\partial x} - \hat{a}_y \varepsilon_y(x, y) \frac{\partial \phi(x, y)}{\partial y} \right] = \rho_v \tag{2}$$

where $\hat{a}_x$ and $\hat{a}_y$ are unit vectors in the x and y directions, respectively, and ρ_v is the charge density distribution. In (2), although ρ_v is equal to zero in the dielectric region, it is reserved for the sake of generality. If the outer conductor is grounded and the inner conductor is at potential V_0, the boundary conditions of (2) are

$$\phi(x, y) = \begin{cases} V_0, & \text{on the inner conductor} \\ 0, & \text{on the outer conductor.} \end{cases} \tag{3}$$

When the dielectric medium is homogeneous, (2) can be simplified to the well-known Poisson's equation as given by

$$\varepsilon_x \frac{\partial^2 \phi}{\partial x^2} + \varepsilon_y \frac{\partial^2 \phi}{\partial y^2} = -\rho_V. \tag{4}$$

An alternative derivation of the governing equation for the electric potential distribution is in the form of an integral equation. Fig. 2(a) shows a typical dielectric region where a control surface encloses a shaded control volume V. This control volume is the rectangle $x_2 \le x \le x_4$, $y_2 \le y \le y_4$. Obviously, this control surface consists of the east, south, west, and north faces, which are denoted as S_e, S_s, S_w, and S_n, respectively. Integrating (2) over the control volume and applying the divergence theorem gives the Gauss law

$$\int_{S_e} \varepsilon_x \frac{-\partial \phi}{\partial x}\, dy + \int_{S_w} \varepsilon_x \frac{\partial \phi}{\partial x}\, dy + \int_{S_n} \varepsilon_y \frac{-\partial \phi}{\partial y}\, dx + \int_{S_s} \varepsilon_y \frac{\partial \phi}{\partial y}\, dx = \int_V \rho_v\, dV. \tag{5}$$

The first, second, third, and fourth surface integrals in the left-hand side (LHS) of (5), referred to as the electric fluxes flowing

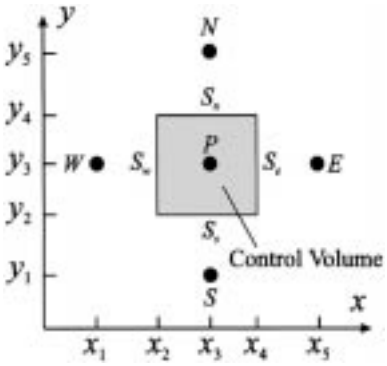

(a)

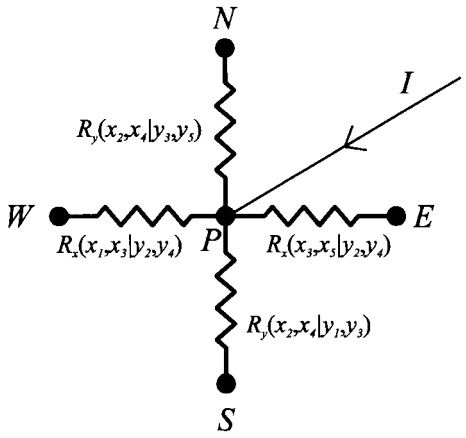

(b)

Fig. 2. (a) Control volume used for finite-volume discretization method. (b) Circuit analogy of the finite-difference form at point P.

through the east, west, north, and south faces of the control volume, are denoted as ψ_e, ψ_w, ψ_n, and ψ_s, respectively. The right-hand side (RHS) of (5) is the total charge Q in the control volume V.

III. Discretization of the Computational Domain

Before constructing computational grid points, the computational domain is divided into a group of subcells. As depicted in Fig. 1, the entire computational domain in this calculation is initially divided into 3×2 cells, which is defined as the coarsest level $k = 1$. This is the simplest dividing method which can represent the conductor-to-dielectric interfaces. Then, equally dividing each cell on level $k = 1$ into four finer subcells regardless of the dielectric boundaries gives 6×4 subcells on level $k = 2$ as shown in Fig. 3. This fining process is continued until the refinement is sufficient for the required accuracy on the finest level $k = M$. Hence, there are $N_x^{(k)} \times N_y^{(k)}$ subcells on level k, where $N_x^{(k)} = 3 \cdot 2^{k-1}$ and $N_y^{(k)} = 2 \cdot 2^{k-1}$.

A vertex-centered grid or a cell-centered grid can be used to discretize the computational domain. In the vertex-centered case, the computational grid is composed of a finite set of grid points which are located at the vertices of the cells. In this paper, a cell-centered grid, which constructs the computational grid points at the centers of the cells is used to discretize the computational domain. The cell-centered grids, from the coarsest to the finest levels, are defined as $G^{(1)}$, $\cdots$, $G^{(k)}$, $\cdots$, $G^{(M)}$, respectively. Hence, the grid $G^{(k)}$ is composed of $N_x^{(k)} \times N_y^{(k)}$ grid points. Fig. 3 shows the cell-centered grids $G^{(1)}$ and $G^{(2)}$. The coarsest grid $G^{(1)}$ includes 3×2 grid points and the finer grid $G^{(2)}$ includes 6×4 grid points. It should be noted that each cell on the finest level may or may not include different dielectrics while discretizing the computational domain. Hence, this strategy is more flexible than the conventionally used vertex-centered method [9]–[13], which should locate the computational grid points at the dielectric boundaries.

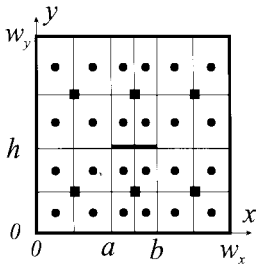

Fig. 3. Cell-centered grids on $G^{(1)}$ and $G^{(2)}$. ■ represents grid points on $G^{(1)}$, and • represents grid points on $G^{(2)}$.

IV. Discretization of the Governing Equations

A typical computational grid point $P(x_3, y_3)$ surrounded by four adjacent grid points $E(x_5, y_3)$, $S(x_3, y_1)$, $W(x_1, y_3)$, and $N(x_3, y_5)$ is shown in Fig. 2(a). Let ϕ_P, ϕ_E, ϕ_S, ϕ_W, and ϕ_N be the potentials at grid points P, E, S, W, and N, respectively. The goal of this section is to derive the relation between ϕ_P, ϕ_E, ϕ_S, ϕ_W, and ϕ_N. Many authors [9]–[13] use a vertex-centered grid to discretize the computational domain and transform the differential equations (2) or (4) into finite-difference forms at each grid point by replacing the derivatives in (2) or (4) by truncated Taylor's series. However, the normal derivative of the electric potential is discontinuous at the interface between two different dielectric media. Hence, this strategy from discretizing the differential equation is difficult to be implemented, for example, if there are two different dielectric media between points P and E. To overcome this difficulty, the finite-volume discretization, which sets forth from discretizing the integral (5), is used. Integrating the x-directed component electric field from point (x_3, y) to point (x_5, y) [cf. Fig. 2(a)] gives

$$\phi(x_3, y) - \phi(x_5, y) = \int_{x_3}^{x_5} \frac{D_x(x, y)}{\varepsilon_x(x, y)}\, dx, \qquad y_2 \le y \le y_4 \tag{6}$$

where D_x is the x-directed electric induction. Although ε_x may pose discontinuity at the interface between points (x_3, y) and (x_5, y), D_x is continuous at this interface whose normal vector is assumed to be parallel to $\hat{a}_x$. Hence, it is reasonable to approximate $D_x(x, y)$ in (6) by its value at point (x_4, y) if the distance between points P and E is small enough. Substituting the approximate $D_x(x_4, y)$ in (6) into the first surface integral

in (5) gives

$$\psi_e = \int_{y_2}^{y_4} D_x(x_4, y)\, dy = \int_{y_2}^{y_4} \frac{\phi(x_3, y) - \phi(x_5, y)}{\displaystyle\int_{x_3}^{x_5} \frac{1}{\varepsilon_x(x, y)}\, dx}\, dy. \quad (7)$$

Approximating $\phi(x_3, y)$ by ϕ_P and $\phi(x_5, y)$ by ϕ_E (assume the control volume is small enough), ψ_e can be expressed as a function of ϕ_P and ϕ_E. Similarly, ψ_w can be expressed as a function of ϕ_P and ϕ_W, ψ_n as a function of ϕ_P and ϕ_N, and ψ_s as a function of ϕ_P and ϕ_S. Then, substituting ψ_e, ψ_w, ψ_s, and ψ_n into (5) gives the discretization form of the integral (5) at point P

$$\begin{aligned}
&\varepsilon_x^{eq}(x_3, x_5|y_2, y_4)\, \frac{\phi_P - \phi_E}{x_5 - x_3}\, (y_4 - y_2) \\
&\quad + \varepsilon_x^{eq}(x_1, x_3|y_2, y_4)\, \frac{\phi_P - \phi_W}{x_3 - x_1}\, (y_4 - y_2) \\
&\quad + \varepsilon_y^{eq}(x_2, x_4|y_3, y_5)\, \frac{\phi_P - \phi_N}{y_5 - y_3}\, (x_4 - x_2) \\
&\quad + \varepsilon_y^{eq}(x_2, x_4|y_1, y_3)\, \frac{\phi_P - \phi_S}{y_3 - y_1}\, (x_4 - x_2) = Q \quad (8)
\end{aligned}$$

where the functions ε_x^{eq} and ε_y^{eq} are defined as the functions

$$\begin{aligned}
&\varepsilon_x^{eq}(x_a, x_b|y_c, y_d) \\
&\quad = \frac{1}{y_d - y_c} \int_{y_c}^{y_d} \frac{1}{\dfrac{1}{x_b - x_a} \displaystyle\int_{x_a}^{x_b} \frac{1}{\varepsilon_x(x, y)}\, dx}\, dy \quad (9)
\end{aligned}$$

and

$$\begin{aligned}
&\varepsilon_y^{eq}(x_a, x_b|y_c, y_d) \\
&\quad = \frac{1}{x_b - x_a} \int_{x_a}^{x_b} \frac{1}{\dfrac{1}{y_d - y_c} \displaystyle\int_{y_c}^{y_d} \frac{1}{\varepsilon_y(x, y)}\, dy}\, dx \quad (10)
\end{aligned}$$

respectively. Note that, $\varepsilon_x^{eq}(x_a, x_b|y_c, y_d)$ [or $\varepsilon_y^{eq}(x_a, , x_b|y_c, y_d)$], referred to as the equivalent dielectric constant for the flux flowing in the horizontal (or vertical) direction of the rectangle $x_a \le x \le x_b$, $y_c \le y \le y_d$, is obtained by taking the harmonic average of ε_x (or ε_y) in the interval $x_a \le x \le x_b$ (or $y_c \le y \le y_d$), then taking the arithmetic average of the previous result in the interval $y_c \le y \le y_d$ (or $x_a \le x \le x_b$).

V. Circuit Analogy of the Finite-Volume Discretization

As the governing equations of quasi-static and steady current problems are essentially the same in mathematics, the analyses of them are in close analogy to each other with the dual quantities defined in Table I. Hence, it is possible to illustrate the mathematical derivation of the difference equation in Section IV by a simple but meaningful resistive network model. To obtain this goal, the general finite-difference form (8) at point P can be rewritten as Kirchhoff's current law at point P [see Fig. 2(b)]

$$\begin{aligned}
&\frac{\phi_P - \phi_E}{R_x(x_3, x_5|y_2, y_4)} + \frac{\phi_P - \phi_W}{R_x(x_1, x_3|y_2, y_4)} \\
&\quad + \frac{\phi_P - \phi_N}{R_y(x_2, x_4|y_3, y_5)} + \frac{\phi_P - \phi_S}{R_y(x_2, x_4|y_1, y_3)} = I \quad (11)
\end{aligned}$$

TABLE I
Analogy Between Quasi-Static and Steady Current Problems

Quasi-Static Problem	Steady Current Problem
electric potential distribution $\phi(x,y)$	electric potential distribution $\phi(x,y)$
electric field distribution $\vec{E}(x,y)$	electric field distribution $\vec{E}(x,y)$
electric flux density $\vec{D}$	current density $\vec{J}$
differential equation $\nabla \cdot \vec{D} = \rho_r$	differential equation $\nabla \cdot \vec{J} = 0$
constitutive relation $\vec{D} = [\varepsilon]\vec{E}$	Ohm's law $\vec{J} = \sigma\vec{E}$
dielectric constant ε	conductivity σ
electric flux ψ or charge Q	current I
capacitance C	conductance $1/R$
Gauss' law	Kirchhoff's current law

where R_x and R_y are defined as the functions

$$\begin{aligned}
R_x(x_a, x_b|y_c, y_d) &= \frac{x_b - x_a}{\varepsilon_x^{eq}(x_a, x_b|y_c, y_d)(y_d - y_c)} \\
&= \frac{1}{\displaystyle\int_{y_c}^{y_d} \frac{1}{\displaystyle\int_{x_a}^{x_b} \frac{1}{\varepsilon_x(x, y)}\, dx}\, dy} \quad (12)
\end{aligned}$$

and

$$\begin{aligned}
R_y(x_a, x_b|y_c, y_d) &= \frac{y_d - y_c}{\varepsilon_y^{eq}(x_a, x_b|y_c, y_d)(x_b - x_a)} \\
&= \frac{1}{\displaystyle\int_{x_a}^{x_b} \frac{1}{\displaystyle\int_{y_c}^{y_d} \frac{1}{\varepsilon_y(x, y)}\, dy}\, dx} \quad (13)
\end{aligned}$$

respectively. In (11), I, which is actually the Q in (8), is referred to as the current source at point P. In (12) [or (13)], $R_x(x_a, x_b|y_c, y_d)$ [or $R_y(x_a, x_b|y_c, y_d)$] is referred to as the equivalent resistance for the current flowing in the horizontal (or vertical) direction of the rectangle $x_a \le x \le x_b$, $y_c \le y \le y_d$. In general, the analytical solutions of the integrations in $R_x(x_a, x_b|y_c, y_d)$ and $R_y(x_a, x_b|y_c, y_d)$ are not available and numerical calculations are needed. To speed up the calculation, the simple midpoint integration formula is adopted. For example, if ε_x is smooth in the rectangle $x_a \le x \le x_b$, $y_c \le y \le y_d$, $\varepsilon_x^{eq}(x_a, x_b|y_c, y_d)$ in (12) is approximated by ε_x at point $[(x_a + x_b)/2, (y_c + y_d)/2]$. On the other hand, if ε_x poses discontinuities in this rectangle, the midpoint integration formula is applied on each smooth subregions. Moreover, if ε_x and ε_y are constant, the general finite-difference form at point P, as derived in (11), is simplified to the standard five-point difference approximation of Poisson's equation [9]–[13].

Now, consider the $N_x^{(M)} \times N_y^{(M)}$ cells on the finest level. A typical cell (shaded region) is enlarged as shown in Fig. 4. When this cell doesn't border any conductor, applying the general finite-difference form (11) at point P and choosing the control volume just as this shaded cell gives the discretization form of the integral equation (5) at point P. When the boundary of the shaded cell borders the conductor,

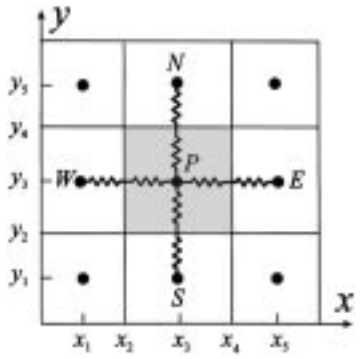

Fig. 4. A local enlargement of the cell-centered grid $G^{(M)}$ and its circuit analogy.

the Dirichlet boundary condition should be applied, so (11) should be slightly modified. For example, when the north side of the shaded cell borders the inner conductor, ϕ_N and $R_y(x_2, x_4|y_3, y_5)$ in (11) should be replaced by V_0 and $R_y(x_2, x_4|y_3, y_4)$, respectively. If the integration in the interval $y_2 \le y \le y_4$ is approximated by the midpoint integration formula, $R_x(x_3, x_5|y_2, y_4)$ can be regarded as the series of two lump resistors $R_x(x_3, x_4|y_2, y_4)$ and $R_x(x_4, x_5|y_2, y_4)$

$$R_x(x_3, x_5|y_2, y_4) = R_x(x_3, x_4|y_2, y_4) + R_x(x_4, x_5|y_2, y_4). \tag{14}$$

Hence, in the numerical calculation, as depicted in Fig. 4, one should prepare four *resistances* $R_x(x_3, x_4|y_2, y_4)$, $R_x(x_2, x_3|y_2, y_4)$, $R_y(x_2, x_4|y_3, y_4)$, and $R_y(x_2, x_4|y_2, y_3)$ for each cell on the finest level. Finally, applying Kirchhoff's current law at each grid point of the finest grid $G^{(M)}$, $N_x^{(M)} \times N_y^{(M)}$ linear algebraic equations can be obtained and are written as the following matrix equation:

$$A^{(M)}\phi^{(M)} = f^{(M)} \tag{15}$$

where $A^{(M)}$ is a matrix, $\phi^{(M)}$ is the unknown vector on $G^{(M)}$, and $f^{(M)}$ is the known vector of the matrix equation. The solution of (15) will be described in the following section.

When the final potential distribution $\phi^{(M)}$ is obtained, the total charge on the inner conductor can be calculated by applying Gauss' law to a control surface enclosing the inner conductor. The control volume is a rectangle with the control surfaces coincident with the boundaries or the cells on the finest level. The total charge on the inner conductor Q_{in} is equal to the *total current* flowing out of the control surface. Since the finite-volume discretization preserves the conservation of the electric flux, the calculated total charge on the inner conductor is independent of the position of the control volume. Then, the capacitance can be obtained by calculating Q_{in}/V_0.

VI. The Multigrid Method

A. Multigrid Algorithm

The matrix (15) is banded and sparse, and can be solved by the conventional iteration methods such as GS, red–black GS, and successive over-relaxation method, etc. However, the conventional iteration methods, which do iteration on the single grid (i.e., the finest grid) all suffer from the problem of poor convergence. Owing to these iteration methods are to correct the potential distribution point by point, the high-frequency (HF) components of error are then rapidly reduced (smoothed) and the low-frequency components are difficult to be removed. Hence, in the real calculation, the convergence is fast for the first two or three iterations; then the convergence becomes very slow for the remaining iterations.

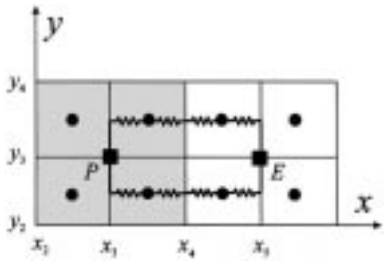

Fig. 5. A local enlargement of the cell-centered grids $G^{(M)}$ and $G^{(M-1)}$ and its circuit analogy. • represents grid points on $G^{(M)}$ and ■ represents grid points on $G^{(M-1)}$.

The slow convergence of iteration on a single grid can be improved by introducing the multigrid method. The basic idea of the multigrid method is to iterate not on a single grid, but on a sequence of fining grids. Hence, the higher frequency-error components can be reduced by iteration on finer grids and the lower frequency-error components can be reduced by iteration on coarser grids. For simplicity, the two-grid method, a special case of the multigrid method, is considered, first. One iteration cycle for the two-grid method, which does iteration on $G^{(M)}$ and $G^{(M-1)}$ (cf. Fig. 5), is loosely described as the following steps [20].

1) Applying a few, e.g., two or three, GS iterations on (15) with a suitable initial guess gives the approximate solution $\phi_*^{(M)}$. Then, the error $e^{(M)} \equiv \phi^{(M)} - \phi_*^{(M)}$, which is mainly composed of low-frequency components, should satisfy the following defect equation:

$$A^{(M)}e^{(M)} = r^{(M)} \tag{16}$$

with residual

$$r^{(M)} = f^{(M)} - A^{(M)}\phi_*^{(M)}. \tag{17}$$

It should be noted that (16) is of the same form as (15).

2) Projecting the defect equation from $G^{(M)}$ to $G^{(M-1)}$ gives

$$A^{(M-1)}e^{(M-1)} = r^{(M-1)} \tag{18}$$

where $A^{(M-1)}$ is the coarse-grid operator on $G^{(M-1)}$ and the details will be described in the next subsection, $e^{(M-1)}$ is the unknown error on $G^{(M-1)}$, $r^{(M-1)}$ is obtained by using the bilinear restriction [14] of $r^{(M)}$ from $G^{(M)}$ to $G^{(M-1)}$. Then, applying two or three GS iterations on (18) with a zero initial guess gives the approximate solution $e_*^{(M-1)}$. Now, the HF components of

error on $G^{(M-1)}$, which are low-frequency components relative to $G^{(M)}$, can be reduced. Using an effective area interpolation [19] for $e_*^{(M-1)}$ from $G^{(M-1)}$ to $G^{(M)}$ gives $e_*^{(M)}$ Thus, the new approximate solution $\phi_*^{(M)}$ is replaced by $\phi_*^{(M)} + e_*^{(M)}$.

3) Applying two or three GS iterations on (15) with the initial guess $\phi_*^{(M)}$ gives the updated approximate solution $\phi_*^{(M)}$.

As more frequency components of error can be reduced by iterating on both $G^{(M)}$ and $G^{(M-1)}$ than on only $G^{(M)}$, it is expected that the convergence rate can be increased if the iterations are applied on all the grids from the finest $G^{(M)}$ to the coarsest $G^{(1)}$. In this work, the multigrid V-cycling (MV) and full multigrid V-cycling (FMV) [20] are both used in the authors' calculation.

B. Coarse-Grid Operator of Cell-Centered Discretization

In this subsection, one wants to derive the coarse-grid operator $A^{(M-1)}$ directly from the finest grid operator $A^{(M)}$. Then $A^{(k)}$, where k is decreasing from $M-2$ to 1, can be derived from $A^{(k+1)}$. When the dielectric medium is homogeneous, the finite-difference forms at a fine-grid point and that at a coarse-grid point are the same. However, if the medium in the fine cells are inhomogeneous, the coarse-grid operator and the fine-grid operator are different. Hence, the derivation of the difference formula on coarse grids should be carefully treated. McCormick defines the coarse-grid operator by a variational approach [16]. However, the operator count is time consuming as referred in [19]. In this work, the finite-volume discretization derived in Section IV and its circuit analogy described in Section V can also be applied in this case. The shaded region, which includes four equal fine cells as shown in Fig. 5, is chosen as the control volume. Although the discretization error is larger on the coarser grid than on the finer one, the general finite-difference form (11) is also applied at the coarse-grid point P. That is because the function of the iteration on the coarser grid is simply to reduce the lower frequency components of errors. This mathematical derivation can also be replaced by a resistive network. From (12), $R_x(x_3, x_5|y_2, y_4)$ can be rewritten as

$$R_x(x_3, x_5|y_2, y_4) = \frac{R_x(x_3, x_5|y_2, y_3)\cdot R_x(x_3, x_5|y_3, y_4)}{R_x(x_3, x_5|y_2, y_3) + R_x(x_3, x_5|y_3, y_4)}. \quad (19)$$

By the help of (14), $R_x(x_3, x_5|y_2, y_3)$ and $R_x(x_3, x_5|y_3, y_4)$ in (19) can be rewritten as

$$\begin{aligned} R_x(x_3, x_5|y_2, y_3) &= R_x\left(x_3, \frac{x_3+x_4}{2}\middle|y_2, y_3\right) + R_x\left(\frac{x_3+x_4}{2}, x_4\middle|y_2, y_3\right) \\ &\quad + R_x\left(x_4, \frac{x_4+x_5}{2}\middle|y_2, y_3\right) + R_x\left(\frac{x_4+x_5}{2}, x_5\middle|y_2, y_3\right) \end{aligned} \quad (20)$$

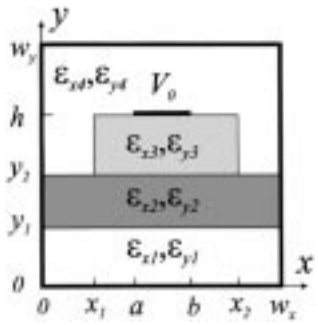

Fig. 6. Microstrip line embedded in an inhomogeneous anisotropic dielectric.

and

$$\begin{aligned} R_x(x_3, x_5|y_3, y_4) &= R_x\left(x_3, \frac{x_3+x_4}{2}\middle|y_3, y_4\right) + R_x\left(\frac{x_3+x_4}{2}, x_4\middle|y_3, y_4\right) \\ &\quad + R_x\left(x_4, \frac{x_4+x_5}{2}\middle|y_3, y_4\right) + R_x\left(\frac{x_4+x_5}{2}, x_5\middle|y_3, y_4\right) \end{aligned} \quad (21)$$

respectively. From (19)–(21), the resistance on $G^{(M-1)}$ can be obtained by the combination of the series and the parallel of the resistance on $G^{(M)}$. Similarly, the resistance on the coarser grid $G^{(k)}$, where k is decreasing from $M-2$ to 1, can also be derived by the help of the resistive network on $G^{(k+1)}$. The same process can also be applied in the calculation of the resistance in the other three directions. Thus, the operation count [19] by using (20) and (21) is much less than that using the variational approach.

VII. Numerical Examples

To demonstrate the rapid convergence of the improved multigrid method proposed in this paper, three examples with the same electrode structures (see Fig. 1) but filled with different dielectric media are tested. The electrode parameters as indicated in Fig. 1 are: $a = 1.2$; $b = 1.8$; $w_x = 3$; $h = 1.2$; and $w_y = 2$. The parameters to be calculated is the capacitance C and the effective dielectric constant ε_{eff}, defined as C/C_o, where C_o is obtained by calculating C with all the dielectric media replaced by air.

The first example is a microstrip line embedded in an inhomogeneous anisotropic dielectric as shown in Fig. 6 [21], [22]. There are four kinds of anisotropic dielectric medium enclosed by the conducting boundary. Each dielectric has a dielectric constant, and therefore, the dielectric medium is globally inhomogeneous. First, the isotropic case is considered. The parameters as indicated in the figure for the numerical test are $x_1 = 0.8$, $x_2 = 2.2$, $y_1 = 0.4$, $y_2 = 0.8$, $\varepsilon_{x1} = \varepsilon_{y1} = \varepsilon_0$, $\varepsilon_{x2} = \varepsilon_{y2} = 6\varepsilon_0$, $\varepsilon_{x3} = \varepsilon_{y3} = 10\varepsilon_0$, $\varepsilon_{x4} = \varepsilon_{y4} = \varepsilon_0$, where ε_0 is the dielectric constant of air. Fig. 7(a) shows the normalized L_2 norm of residual on $G^{(6)}$ for three iteration methods: FMV, MV [20], and GS on the finest grid $G^{(6)}$. Solid and dashed lines denote the cases with and without dielectrics, respectively. The costs of the above three iterations are measured in terms of work units. One work unit $WU^{(M)}$

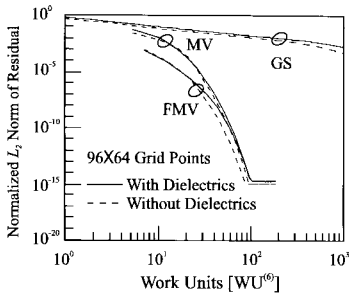

(a)

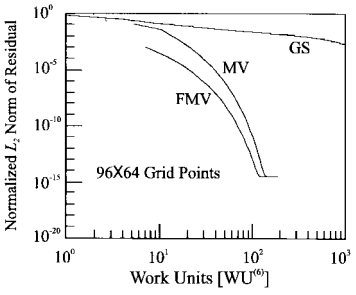

(b)

Fig. 7. Convergence history of the normalized L_2 norm of the residual for microstrip line shown in Fig. 6. (a) Isotropic and (b) anisotropic dielectric medium.

TABLE II
NUMBER OF WORK UNITS REQUIRED FOR THE FIRST EXAMPLE

Grid Points	Work Units	Without Dielectrics			With Dielectrics					
					Isotropic			Anisotropic		
		FMV	MV	GS	FMV	MV	GS	FMV	MV	GS
6×4	$[WU^{(2)}]$	28.5	32.5	22	35.0	32.5	32	35.0	32.5	43
12×8	$[WU^{(3)}]$	30.4	28.1	73	24.8	28.1	101	24.8	28.1	68
24×16	$[WU^{(4)}]$	29.0	32.4	256	29.0	32.4	372	29.0	37.8	353
48×32	$[WU^{(5)}]$	28.6	32.1	913	28.6	37.5	1199	34.0	48.2	1021
96×64	$[WU^{(6)}]$	28.5	37.4	3249	28.5	37.4	4771	33.8	53.4	4085
192×128	$[WU^{(7)}]$	23.1	37.3		23.1	37.3		33.8	53.3	

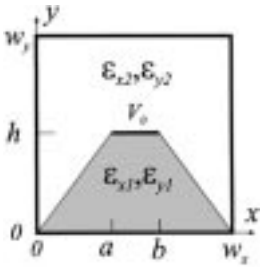

Fig. 8. Microstrip line with slope sidewall embedded in an anisotropic dielectric.

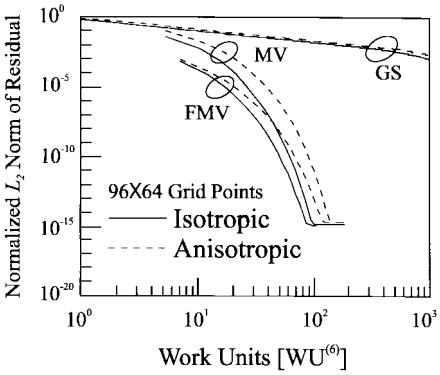

Fig. 9. Convergence history of the normalized L_2 norm of the residual for the microstrip line shown in Fig. 8.

denotes the cost of performing one GS iteration on the finest grid $G^{(M)}$ [19]. Table II shows the number of work units required for a normalized L_2 norm of less than or equal to 10^{-6}. Obviously, the convergence rate of the GS scheme is extremely poor as compared to those of the FMV and MV. This is because the low-frequency components of error are difficult to be removed by the conventional GS method, which iterates only on a single grid (finest grid). The convergence rate of the FMV is slightly faster than that of the MV because a better initial guess on $G^{(M)}$ is adopted by the FMV [20]. As can also be seen from Fig. 7(a) and Table II, the convergence rate in the calculation of the field distribution with and without dielectrics are quite similar, which indicates the complexity of dielectric structure only slightly affects the convergence rate during iteration. To test the convergence rate for the anisotropic case, the previous dielectric constants are replaced by $\varepsilon_{x1} = 3\varepsilon_0$, $\varepsilon_{y1} = 6\varepsilon_0$, $\varepsilon_{x2} = 6\varepsilon_0$, $\varepsilon_{y2} = 10\varepsilon_0$, $\varepsilon_{x3} = 43\varepsilon_0$, $\varepsilon_{y2} = 28\varepsilon_0$, and $\varepsilon_{x4} = \varepsilon_{y4} = \varepsilon_0$. The same calculation is also carried out once again. The results are shown in Fig. 7(b) and Table II. Similar fast convergence is also obtained. And the anisotropy of the dielectric does not significantly affect the convergence rate, too.

The second example is to analyze the microstrip line as shown in Fig. 8. In this example, the sidewall of the dielectric medium has a slope, which can be found in the fabrication of the integrated optical waveguide [23], [24]. The slope makes the problem much more difficult to be solved by the conventional vertex-centered finite-difference method. The parameters used for the isotropic case are $\varepsilon_{x1} = \varepsilon_{y1} = 10\varepsilon_0$ and $\varepsilon_{x2} = \varepsilon_{y2} = \varepsilon_0$, $\varepsilon_{y2} = 10\varepsilon_0$. For the anisotropic case, the parameters are $\varepsilon_{x1} = 43\varepsilon_0$, $\varepsilon_{y1} = 28\varepsilon_0$, and $\varepsilon_{x2} = \varepsilon_{y2} = \varepsilon_0$. The dielectric constants are assumed to be staircase near the slope. Hence, the normal vectors of the interfaces where the dielectric constants pose discontinuity are still parallel to the x- or y-axis. Fig. 9 shows the normalized L_2 norm of residual calculated by FMV, MV, and GS methods of iterations used previously. Table III also shows the number of work units required for a normalized L_2 norm of less than or equal to 10^{-6}. As can be seen from Fig. 9 and Table III, the improved multigrid method also works as well for this case. Again, no significant difference in rates of convergence due to the anisotropy of the structure is observed.

To demonstrate the convergence rate for a more complicated dielectric structure, the third example is depicted as shown in Fig. 10. The dielectric constant is graded in the substrate as given by

$$\varepsilon_{x1} = \varepsilon_0 + \Delta\varepsilon_{rx}\varepsilon_0 e^{-[(x-c)/c^2]} e^{-[(y-h)/h]^2} \quad (22.1)$$

$$\varepsilon_{y1} = \varepsilon_0 + \Delta\varepsilon_{ry}\varepsilon_0 e^{-[(x-c)/c]^2} e^{-[(y-h)/h]^2} \quad (22.2)$$

TABLE III
NUMBER OF WORK UNITS REQUIRED FOR THE SECOND EXAMPLE

Grid Points	Work Units	Isotropic Dielectric			Anisotropic Dielectric		
		FMV	MV	GS	FMV	MV	GS
6×4	$[WU^{(2)}]$	28.5	26.0	26	35.0	39.0	35
12×8	$[WU^{(3)}]$	30.4	28.1	83	36.0	39.4	111
24×16	$[WU^{(4)}]$	29.0	32.4	292	39.8	43.3	392
48×32	$[WU^{(5)}]$	28.6	32.1	1052	34.0	48.2	1413
96×64	$[WU^{(6)}]$	28.5	37.4	3778	33.8	53.4	5083
192×128	$[WU^{(7)}]$	23.1	37.3		28.5	53.3	

TABLE IV
NUMBER OF WORK UNITS REQUIRED FOR THE THIRD EXAMPLE

Grid Points	Work Units	Isotropic Dielectric			Anisotropic Dielectric		
		FMV	MV	GS	FMV	MV	GS
6×4	$[WU^{(2)}]$	22.0	26.0	26	28.5	32.5	32
12×8	$[WU^{(3)}]$	30.4	28.1	88	30.4	33.8	113
24×16	$[WU^{(4)}]$	29.0	32.4	316	39.8	43.3	405
48×32	$[WU^{(5)}]$	28.6	32.1	1135	34.0	48.2	1459
96×64	$[WU^{(6)}]$	28.5	37.4	4059	33.8	53.4	5229
192×128	$[WU^{(7)}]$	28.5	53.3		28.5	53.3	

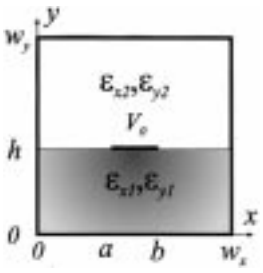

Fig. 10. Microstrip line embedded in an inhomogeneous anisotropic dielectric.

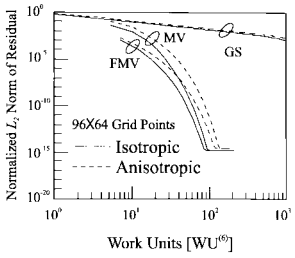

Fig. 11. Convergence history of the normalized L_2 norm of the residual for microstrip line shown in Fig. 10.

where $c = (a + b)/2$. The parameters for the isotropic case as indicated in Fig. 10 for the numerical test are $\Delta\varepsilon_{rx} = \Delta\varepsilon_{rx} = 6$ and $\varepsilon_{x2} = \varepsilon_{y2} = \varepsilon_0$. For the anisotropic case, the parameters are $\Delta\varepsilon_{rx} = 43$ and $\Delta\varepsilon_{ry} = 28$, while ε_{x2} and ε_{y2} are unchanged. Similar fast convergence rate in terms of work units is observed as shown in Fig. 11 and Table IV. Hence, the complexity and the anisotropy of dielectric structure can only have a negligible effect on the convergence rate of the improved multigrid method.

As can also been seen from Tables II–IV, to obtain certain required accuracy, the work units [in terms of $WU^{(M)}$] required for FMV or MV iterations on $G^{(M)}$ are almost the same for all M, while that for GS iterations is increasing rapidly with M. Note that the cost of one work unit $WU^{(k)}$ is four times as large as one work unit $WU^{(k-1)}$ since the number of grid points on $G^{(k)}$ is four times as those on $G^{(k-1)}$. Thus, the computing time for the FMV and MV are approximately on the order of $O(N_p)$, where N_p is the number of grid points, but roughly on the order of $O(N_p^2)$ for GS iterations. So, the FMV and MV are most suitable for the problem with a large amount grid points, where the iterations required for the GS is extremely large.

TABLE V
EFFECTIVE DIELECTRIC CONSTANTS

Example		Effective Dielectric Constant	
		This method	[7] and [8]
Ex1	Isotropic	2.7517	2.7570
	Anisotropic	6.0619	
Ex2	Isotropic	4.1449	4.0868
	Anisotropic	10.8515	
Ex3	Isotropic	3.1213	
	Anisotropic	12.4150	

The effective dielectric constants calculated by the FMV in the above three examples are shown in Table V. The difference between the results calculated by this method and that obtained by the moment method [7], [8] is less than 2%.

VIII. CONCLUSION

An improved multigrid technique has been successfully applied in the quasi-TEM analysis of a microstrip embedded in an inhomogeneous anisotropic medium. The general finite-difference form on inhomogeneous anisotropic medium is derived by the finite-volume discretization of an integral equation, which preserves the conservation of the electric flux. Owing to the close analogy between the quasi-TEM and steady current problems, the solution of the microstrip line embedded in an inhomogeneous anisotropic medium is equivalent to that of a resistive network. The finite-difference forms, from the finest to the coarsest, can all be obtained by applying the Kirchhoff law on the resistive network. The resulting matrix equation for the potential distribution on the finest grid is solved by the improved multigrid iteration, where the coarse-grid operator is derived directly from that on the finest grid by the help of an equivalent resistive network.

Three numerical examples are given and the results are in good agreement with those by the other method when special cases are considered. The convergence rate is hardly dependent of the number of unknowns and the complexity of the dielectric media.

In this paper, only one microstrip line embedded in an inhomogeneous anisotropic medium is considered. However, in many practical applications, two or more microstrip lines are usually involved. The application of the present method on the field calculation of these microstrip structures will be of great interest in the future.

REFERENCES

[1] H. A. Wheeler, "Transmission-line properties of parallel strips separated by a dielectric sheet," *IEEE Trans. Microwave Theory Tech.,* vol. MTT-13, pp. 172–185, Mar. 1965.

[2] O. G. Ramer, "Integrated optics electrooptic modulator electrode analysis," *IEEE J. Quantum Electron.,* vol. QE-18, pp. 386–392, Mar. 1982.

[3] T. Chang and C. Tan, "Analysis of a shielded microstrip line with finite metallization thickness by the boundary element method," *IEEE Trans. Microwave Theory Tech.,* vol. 38, pp. 1130–1132, Aug. 1990.

[4] K. Atsuki and K. Li, "Partial-boundary element method for analysis of striplines with arbitrary cross-sectional dielectric in multi-layered media," *IEEE Trans. Microwave Theory Tech.,* vol. 43, pp. 1153–1161, May 1995.

[5] H. Jin, R. Vahldieck, M. Belanger, and Z. Jacubczyk, "A mode projecting method for the quasi-static analysis of electrooptic device electrodes considering finite metallization thickness and anisotropic substrate," *IEEE J. Quantum Electron.,* vol. 27, pp. 2306–2314, Oct. 1991.

[6] T. Itoh and A. S. Herbert, "A generalized spectral domain analysis for coupled suspended microstriplines with tuning septums," *IEEE Trans. Microwave Theory Tech.,* vol. MTT-26, pp. 820–826, Oct. 1978.

[7] C. Wei, R. F. Harrington, J. R. Mautz, and T. K. Sarkar, "Multiconductor transmission lines in multilayered dielectric media," *IEEE Trans. Microwave Theory Tech.,* vol. MTT-32, pp. 439–449, Apr. 1984.

[8] Y. Naiheng and R. F. Harrington, "Characteristic impedance of transmission lines with arbitrary dielectrics under the TEM approximation," *IEEE Trans. Microwave Theory Tech.,* vol. MTT-34, pp. 472–475, Apr. 1986.

[9] H. E. Green, "The numerical solution of some important transmission-line problems," *IEEE Trans. Microwave Theory Tech.,* vol. MTT-13, pp. 676–692, Sept. 1965.

[10] M. V. Schneider, "Computation of impedance and attenuation of TEM-lines by finite-difference methods," *IEEE Trans. Microwave Theory Tech.,* vol. MTT-13, pp. 793–800, Nov. 1965.

[11] H. E. Stinehelfer, "An accurate calculation of uniform microstrip transmission lines," *IEEE Trans. Microwave Theory Tech.,* vol. MTT-16, pp. 439–444, July 1968.

[12] T. Hatsuda, "Computation of coplanar-type strip-line characteristics by relaxation method and its application to microwave circuits," *IEEE Trans. Microwave Theory Tech.,* vol. MTT-23, pp. 795–802, Oct. 1975.

[13] R. P. Owens, J. E. Aitken, and T. C. Edwards, "Quasi-static characteristics of microstrip on an anisotropic sapphire substrate," *IEEE Trans. Microwave Theory Tech.,* vol. MTT-24, pp. 499–505, Aug. 1976.

[14] P. Wesseling, *An Introduction to Multigrid Methods.* New York: Wiley, 1992.

[15] R. E. Alcouffe, A. Brant, J. E. Dendy, and J. W. Painter, "The multigrid method for the diffusion equation with strongly discontinuous coefficients," *SIAM J. Sci. Stat. Comput.,* vol. 2, pp. 430–454, 1981.

[16] S. F. McCormick and J. W. Ruge, "Multigrid methods for variational problems," *SIAM J. Numer. Anal.,* vol. 19, pp. 924–929, 1982.

[17] W. Hackbusch, *Multigrid Methods and Applications.* Berlin, Germany: Springer-Verlag, 1985.

[18] J. E. Dendy, "Black box multigrid for systems," *Appl. Math. Comput.,* vol. 19, pp. 57–74, 1986.

[19] C. Liu, Z. Liu, and S. McCormick, "An efficient multigrid scheme for elliptic equations with discontinuous coefficients," *Comm. Appl. Num. Meth.,* vol. 8, pp. 621–631, 1992.

[20] S. McCormick, Ed., *Multigrid Methods.* Philadelphia: SIAM Frontiers in Appl. Math. 3, Soc. for Ind. and Appl. Math., 1987.

[21] H. B. Sequeira, J. A. McClintock, B. Young, and T. Itoh, "A millimeter-wave Microslab oscillator," *IEEE Trans. Microwave Theory Tech.,* vol. MTT-34, pp. 1333–1336, Dec. 1986.

[22] W. Wang, D. Chen, H. R. Fetterman, Y. Shi, W. H. Steier, and L. R. Dalton, "40-GHz polymer electrooptic phase modulators," *IEEE Photon. Technol. Lett.,* vol. 7, pp. 638–640, June 1995.

[23] R. S. Cheng, W. L. Chen, and W. S. Wang, "Mach–Zehnder modulators with lithium niobate ridge waveguides fabricated by proton-exchange wet etch and nickel indiffusion," *IEEE Photon. Technol. Lett.,* vol. 7, pp. 1282–1284, Nov. 1995.

[24] W. L. Chen, R. S. Cheng, J. H. Lee, and W. S. Wang, "Lithium niobate ridge waveguides by nickel diffusion and proton-exchanged wet etching," *IEEE Photon. Technol. Lett.,* vol. 7, pp. 1318–1320, Nov. 1995.

Ching-Long Tsai was born in Taipei, Taiwan, R.O.C., on May 17, 1965. He received the B.S. degree in electrical engineering from National Cheng Kung University, R.O.C., in 1988, and the M.S. and Ph.D. degrees in electrical engineering from National Taiwan University, Taipei, Taiwan, R.O.C., in 1990 and 1996, respectively.

His research interests include the analysis and design of microwave integrated circuits and integrated optical waveguide devices.

Way-Seen Wang (M'84) was born on March 11, 1948, in Taipei, Taiwan, R.O.C. He received the B.S. degree in electrical engineering from National Taiwan University, Taipei, Taiwan, R.O.C., in 1970, and the M.S. and Ph.D. degrees from the University of Southern California, Los Angeles, in 1975 and 1979, respectively.

Since 1971, he has been with the Department of Electrical Engineering, National Taiwan University. In 1984, he became a full Professor. His current research interest is on the design and fabrication of lithium niobate optical waveguide devices.

Dr. Wang is a member of URSI and ISHM.